Effect of Silicon in As-Quenched and Quenched & Tempered Low Carbon Martensite

James Johnson[1], Hyun-Jo Jun[2], Nina Fonstein[2], and Charles M. Enloe[3]

[1] Advanced Steel Processing and Products Research Center
Colorado School of Mines
1500 Illinois St, Golden, CO 80401 USA
e-mail: raljohns@mines.edu, web page: www.mines.edu/research/aspprc

[2]ArcelorMittal Global R&D – East Chicago
3001 E Columbus Drive, East Chicago, IN 46312 USA
e-mail: hyun.jun@arcelormittal.com, nina.fonstein@arcelormittal.com

[3]Severstal North America
14661 Rotunda Dr., Dearborn, MI 48120 USA
e-mail: charles.enloe@severstalna.com

Keywords: Martensite, Silicon, Tensile Strength, APT, TEM

ABSTRACT

Federal mandates promote the use of automotive steels with higher yield and tensile strengths, which in turn necessitate a microstructure that contains a high volume fraction of martensite. Increasing the strength of martensite through carbon addition may lead to issues such as delayed fracture and limited spot weldability. Alternative ways to strengthen martensite are therefore of great importance.

The effect of Si content on the mechanical properties and microstructure of as-quenched and tempered low carbon martensite is investigated. Microstructural changes in as-quenched martensite containing 0~2.5% Si were studied utilizing optical microscopy, TEM, and atom probe tomography. When the mechanical properties of the as-quenched steels were normalized for variations in prior austenite grain size and carbon content, martensite strength linearly increased with Si content. It was found that Si decreases tempering kinetics and retards the softening of the steel. The mechanisms that explain the experimental observations will be discussed.

INTRODUCTION

The growing safety and fuel consumption requirements result in dramatic increases in advanced high strength steels applications with complicated automotive part geometries, which leads to additional pressure to increase the strength of steels without sacrificing formability[1, 2]. Dual phase, complex phase, quenched and partitioned, and other ultra-high strength steels contain significant volume fractions of martensite in combination with other phases to reach the desired range of properties of third generation advanced high strength steel[3-7]. The chemistries of these steels often utilize levels of silicon (Si) higher than in the previous high strength sheet steels. Understanding the effect of Si on the martensites present in these microstructures will help to guide future developments of advanced high strength steels.

As-quenched (AQ) martensite strength is often expressed as a summation of different strengthening mechanisms:

$$\sigma_M = \sigma_{Fe} + \sigma_{DD} + \sigma_{Lath} + \sigma_{SS,C} + \sigma_{PAGS} + \sigma_{SS,Sub} \quad (1)$$

where the individual strengthening components are: the intrinsic strength of iron (σ_{Fe}), dislocation density strengthening (σ_{DD}), lath width strengthening (σ_{Lath}), interstitial solid solution strengthening from carbon ($\sigma_{SS,C}$), prior austenite grain size strengthening (σ_{PAGS}), and solid solution strengthening from substitutional alloying elements ($\sigma_{SS,Sub}$). This equation is used as a basic approach to reveal the effect of variations of specific parameters on strength of martensitic steels[8, 9]. Therefore, the first goal for current investigation was to quantify the solid solution strengthening contribution of Si in as quenched martensite.

Unlike the literature on the effects of Si in AQ martensite, there has been significant works on the effect of Si in quenched and tempered (Q&T) steels, starting with Allten and Payson, who first observed the retarding effect of Si on temper softening of steels[10]. Owen's work observed that, for a given time, Si additions increase the temperature at which second stage of tempering, decomposition of retained austenite to cementite, and third stage, decomposition of transition carbides to cementite, occurred[11]. It was suggested that the onset of the third stage of tempering was no longer controlled by the diffusion of carbon (C) to cementite. This change in tempering behavior was considered to contribute to the low equilibrium solubility of Si in cementite. More recent work on cementite precipitation has suggested that Si strongly retards the growth of cementite even at an early stage when cementite growth occurs without Si partitioning[12-14]. Studies which have examined these microstructural changes and the impact on mechanical behavior have primarily been focused on steels with high C contents or steels treated for longer tempering times[10,11,15-18]. Therefore, the second goal of the study is to investigate effects of Si on early microstructural evolution and mechanical properties in short time tempered low C martensites.

METHODS AND MATERIALS

The chemical composition of laboratory heats is listed in Table I. Ingots were hot and cold rolled to a nominal thickness of 1.5 mm. Two tensile specimens were machined transverse to the rolling direction with gage length of 50 mm and width of 12.5 mm. Due to differences in A_{C3} temperatures by variations in Si contents, tensile samples were fully austenitized at either 875 or 1000 ºC for Si contents of 0.0-1.0 wt.% and 1.5-2.5 wt.%, respectively, and then water quenched. Tempering was performed on additional samples at tempering temperatures of 100 , 250, 300, 350, and 420 ºC for 150 s.

Prior austenite grain boundaries were revealed for all alloys using a saturated picric acid etch in water and light optical microscopy (LOM). Grain sizes were determined using ASTM standard E112-10[19]. Advanced characterization of selected 0.0Si and 2.5Si alloys has been performed by X-ray diffraction (XRD) and Transmission Electron Microscope (TEM) using a JEOL JEM-2100. Thin foil samples for TEM were mechanically polished and electro-chemically etched using 8 % $HClO_4$ + 92 % acetic acid solution. Martensite lath widths were measured using a linear intercept method on TEM micrographs. Differences in C distributions between 0Si and 2.5Si steels were analyzed using atom probe tomography (APT) on a Cameca LEAP™ 4000x Si. Atom probe needle specimens were prepared by electropolishing 300 µm by 300 µm by 1 cm blanks to a tip radius of less than 1 µm in a solution of 5 % perchloric acid in acetic acid. Specimens were then milled using a dual beam field emission scanning electron microscope/focused ion beam (FEI Helios Nanolab 600i) to obtain a suitable tip radius of less than 50 nm for analysis. Further analysis parameters for APT are a pulse fraction of 15%, pulse frequency of 200 kHz, an evaporation percentage of 0.5 %, and a sample temperature of 50 K. Chamber pressure was ~5×10^{-11} torr.

Table I – Steel Alloy Contents (wt. %)

wt.%	C	Mn	Si	Nb	Mo	Al	P	S	N
0.0Si	0.147	1.77	0.01	0.019	0.15	0.037	0.008	0.005	0.0055
0.5Si	0.143	1.75	0.50	0.019	0.15	0.050	0.009	0.005	0.0055
1.0Si	0.150	1.77	0.98	0.019	0.15	0.049	0.009	0.004	0.0055
1.5Si	0.151	1.80	1.55	0.017	0.15	0.071	0.008	0.005	0.0050
2.0Si	0.154	1.86	2.02	0.018	0.16	0.067	0.009	0.005	0.0053
2.5Si	0.155	1.86	2.50	0.018	0.16	0.075	0.008	0.005	0.0053

RESULTS

Mechanical Properties

The tensile properties of as quenched low C martensite are presented in Figure 1. Tensile strength (TS) and yield strength (YS) range from 1520 to 1660 MPa, and 1155 to 1260 MPa, respectively. While uniform elongation does not change with increasing Si content, total elongation (TE) increases significantly when Si content is higher than 1.5 wt. %, in spite of higher strength of steel.

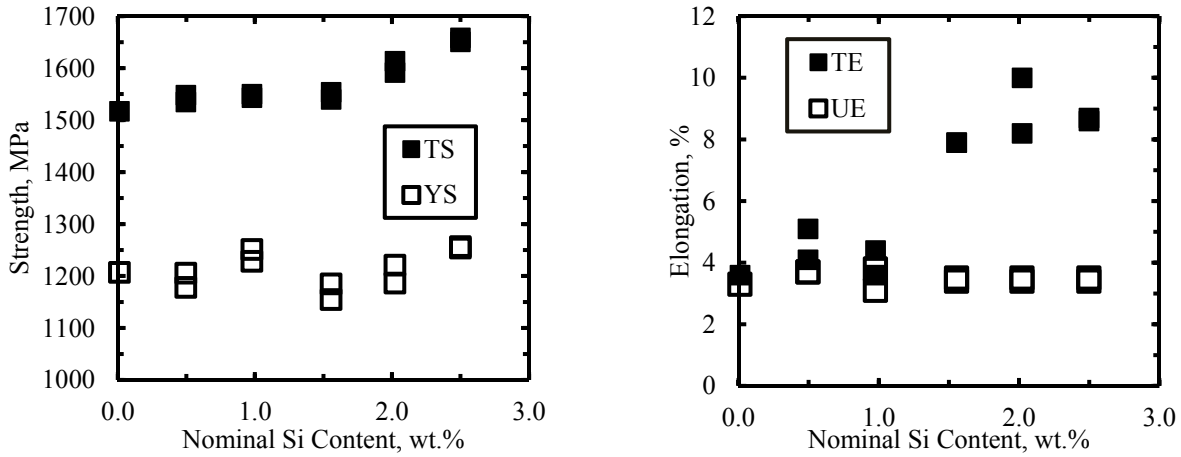

Figure 1. Effect of Si addition on (a) Tensile Strength (TS) and Yield Strength (YE), and (b) Uniform Elongation (UE) and Total Elongation (TE) in AQ martensite.

The TS and YS for the Q&T conditions are presented in Figure 2. The decrease in TS with increasing temper temperature is reduced as the Si content is increased. The YS of the low Si alloys show a similar trend as observed by Nam and Choi in 0.6 wt. % C steel where peaks in YS occur at temperatures near 300 °C[15]. In samples with Si contents greater than the 1.5Si alloy, increases in Si leads only to a gradual increase in YS with increasing temper temperature.

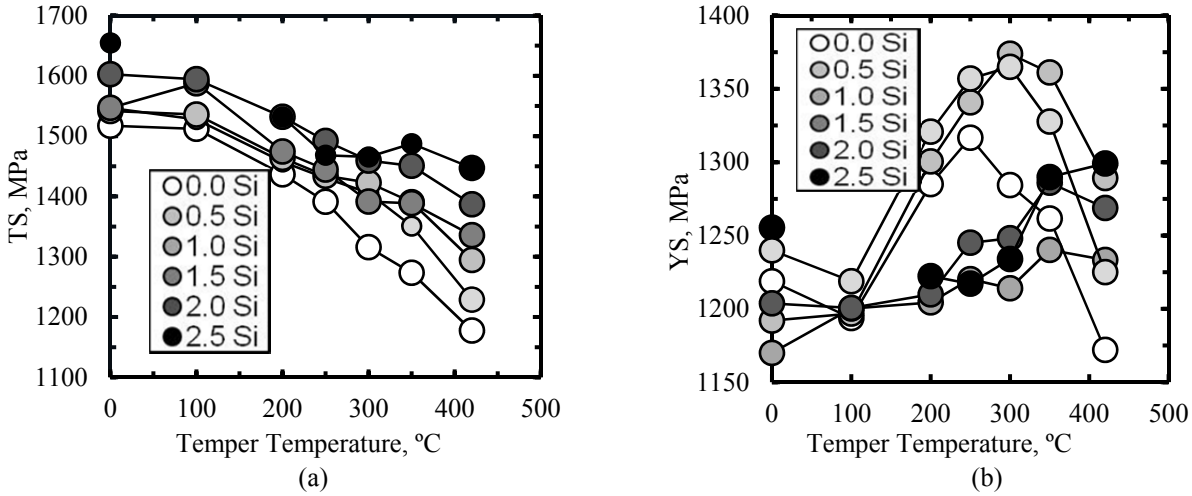

Figure 2. Effect of tempering temperatures (150 s) and Si addition on (a) Tensile Strength (TS) and (b) Yield Strength (YS). The tempering temperature of 0 ºC represents the AQ martensite condition.

The TE for the tempered martensite is shown in Figure 3. The 0.0Si steel shows an increase in TE that peaks at ~7 % at about 200 to 250 °C. In contrast, the TE of the 2.5Si alloy at temperatures above 200 °C ranges from 8 to 10 %. Increases in Si content are thus shown to improve the balance of strength and ductility in the tempered martensite.

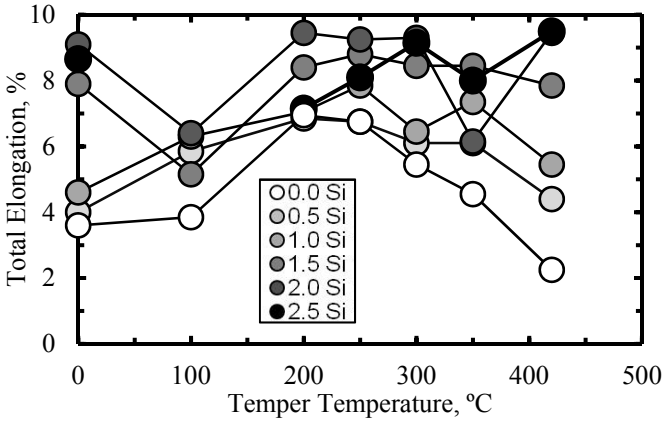

Figure 3. Effect of tempering temperatures (150 s) and Si addition on total elongation in tempered martensite with various Si contents.

Microstructural Characterization

Prior Austenite Grain Size (PAGS) was considered as one of the important strengthening mechanisms of Equation 1 for martensitic steels. Therefore, PAGS was measured in order to isolate the effect of Si addition on AQ martensite strength. The prior austenite grain structure is presented in Figure 4. Results of PAGS measurements are shown in Figure 5. The three low Si alloys have relatively smaller PAGS than in high Si alloys since two different annealing temperatures (875 vs. 1000 °C) were applied to achieve full austenitization due to the variations in Si contents.

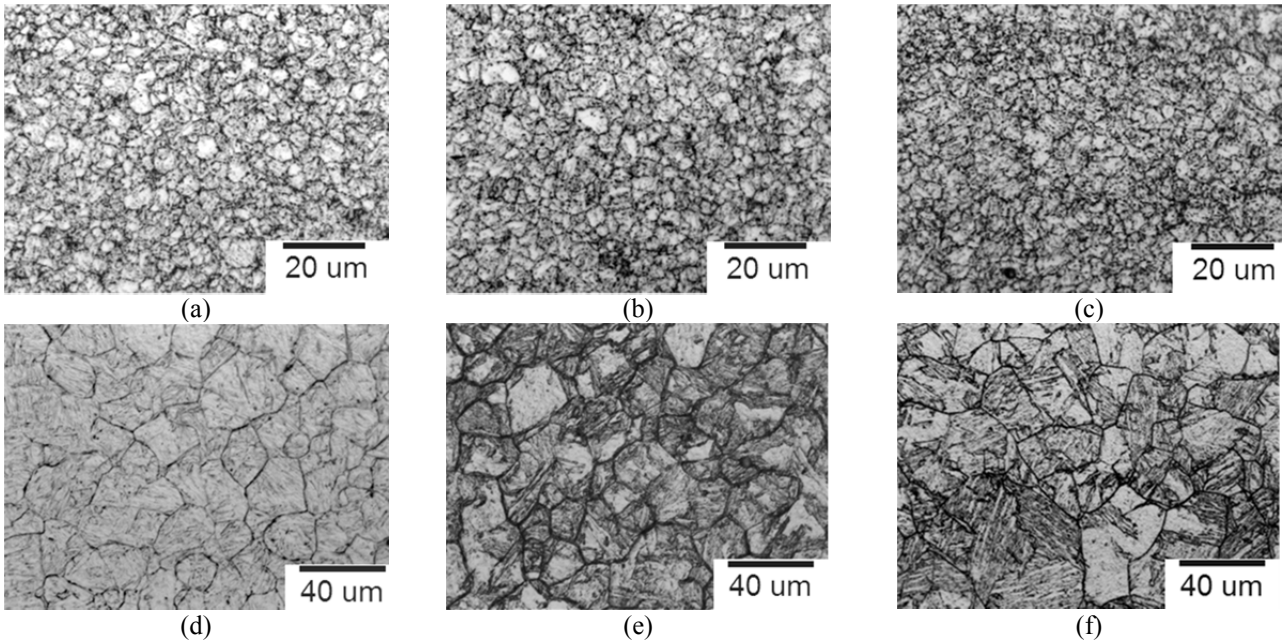

Figure 4. Light optical micrographs showing prior austenite grains: (a) 0.0Si, (b) 0.5Si, (c) 1.0Si, (d) 1.5Si, (e) 2.0Si, and (f) 2.5Si.

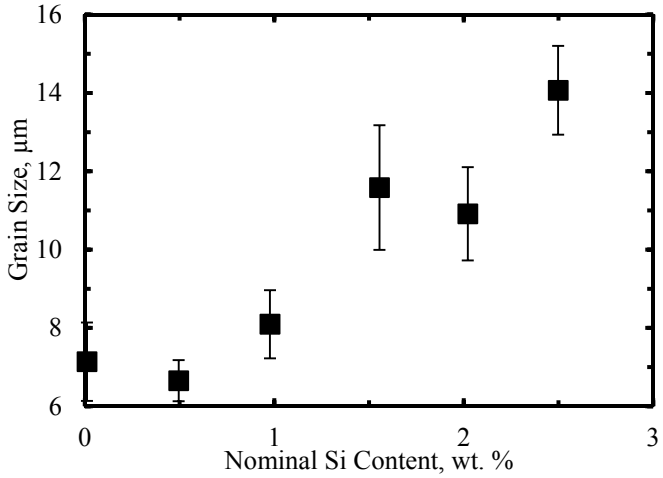

Figure 5. Prior Austenite Grain Size plotted as a function of Si contents. The upper and lower bounds represent 95 % confidence indexes.

Another strengthening factor in martensite is the thickness of lath. The finer lath structure increases the strength of martensite. To determine if differences in Si content might lead to differences in martensite lath structure and strength, bright field TEM observation was performed to examine 0.0Si and 2.5Si AQ specimens as shown in Figure 6 (a) and (d). The average lath widths were measured as 0.27 ±0.1 μm and 0.28 ±0.09 μm for the 0.0Si and 2.5Si alloy, respectively (based on ~350 laths). There is no statistical difference in lath thickness between the two alloys. It should be noted that there no carbides were observed in the AQ martensite of the 0Si and 2.5Si alloys.

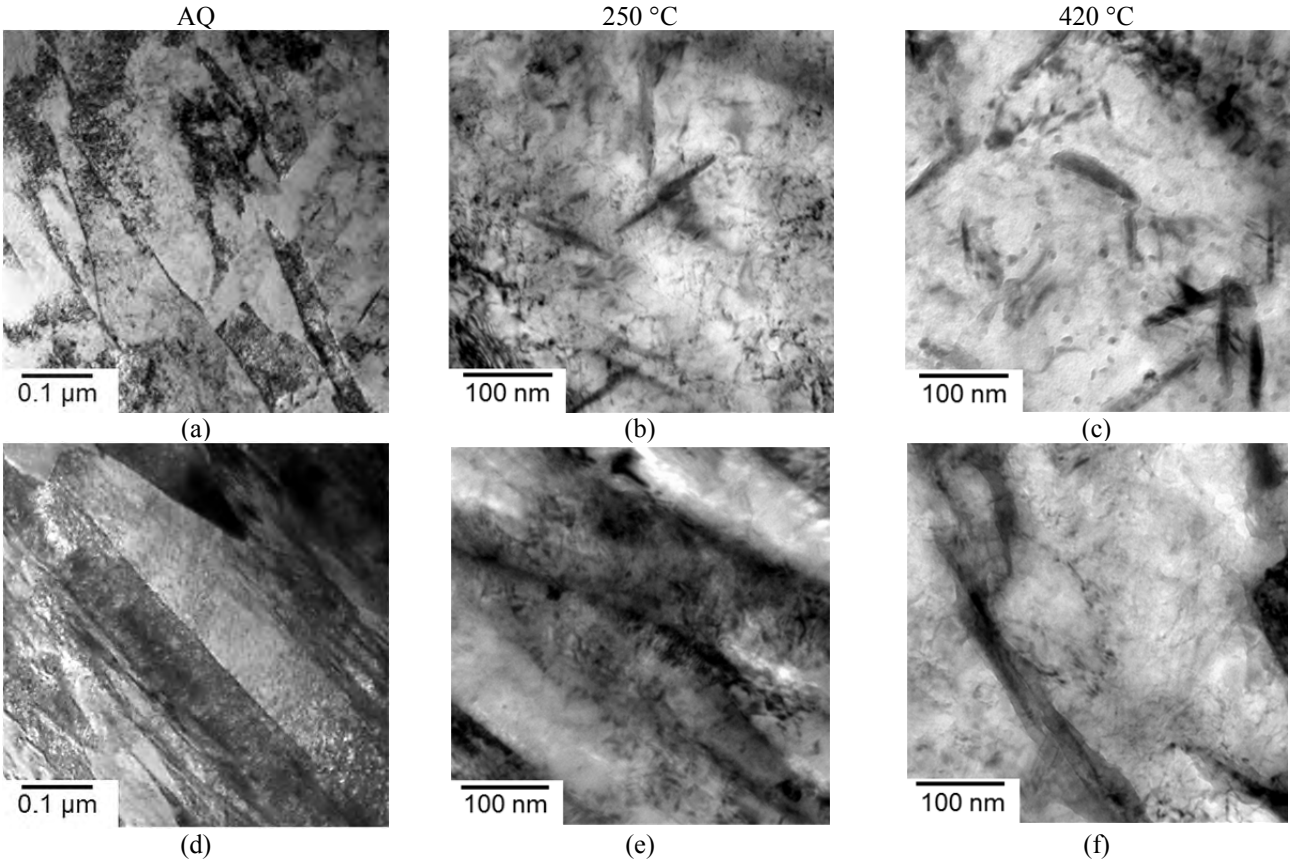

Figure 6. Bright Field TEM micrographs of martensite laths for the 0.0Si (a-c), and 2.5Si (d-f) that were as-quenched (a, d), tempered at 250 ºC (b, e), and tempered at 420 ºC (c, f).

The tempered microstructures of the 0.0Si and 2.5Si steels were also characterized with TEM for the 250 °C and 420 °C tempering temperatures as shown in Figure 6. The 250 °C and 420 °C temperatures were chosen because of the high YS in

the low Si conditions and the most tempered microstructure of the study were obtained, respectively. Upon tempering of the 0.0Si steel, elongated tempering carbides are observed in both tempering temperatures as shown in Figure 6 (b). As tempering temperature increased, the size and amount of these carbides increased, Figure 6(c). In contrast, temper carbides were only observed at the tempering temperature of 420 ºC for the 2.5Si alloy, which is not elongated one like 0Si alloy, Figure 6(f).

To determine if Si had any effect on C distribution/clustering in AQ martensite, APT was performed on specimens from the 0.0Si and 2.5Si alloys. Carbon atom maps for two needles are shown in Figure 7. The average C concentration plotted in Figure 8 is related to the distance either inside or outside of the C iso-concentration surface. However, there is no significant difference in the C gradients around regions of higher carbon content. Comparison of Figure 7 (a) and (b) confirms that Si additions do not result in any significant changes of C distributions in AQ martensite. Additionally, in Figure 7 it is demonstrated that even away from the C clusters, the matrix C concentration does not change with differences in Si contents.

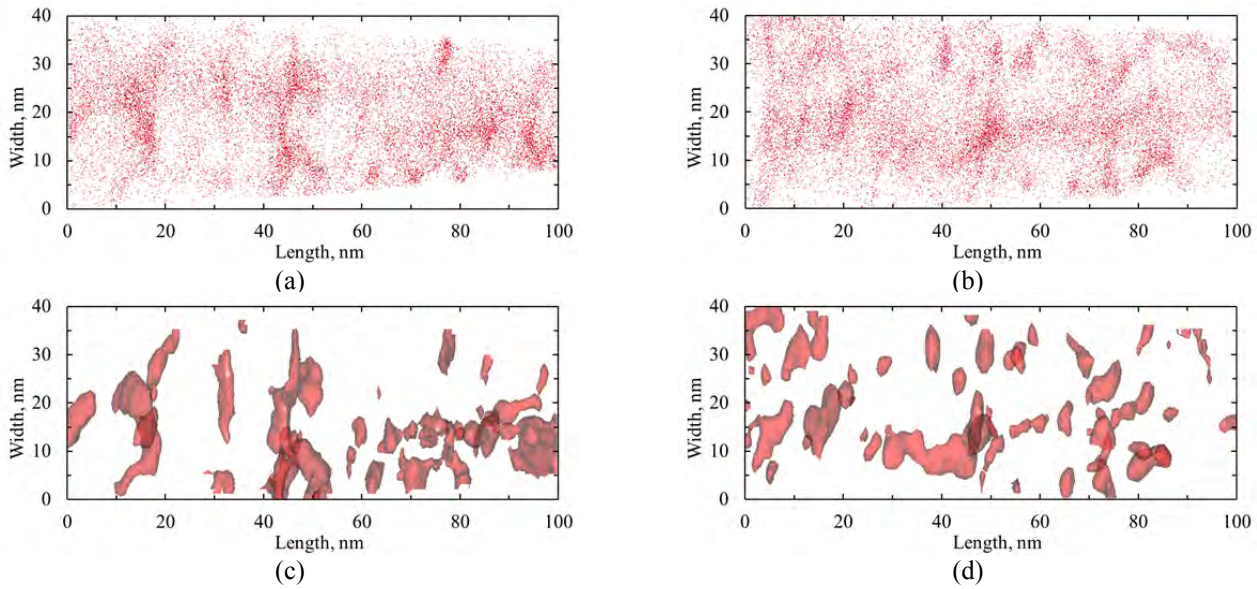

Figure 7. APT C atom map (a, b) and 3 at.% C Iso-concentration Surface (c, d) for 0.0Si (a, c) and 2.5Si (b, d) in the AQ martensite.

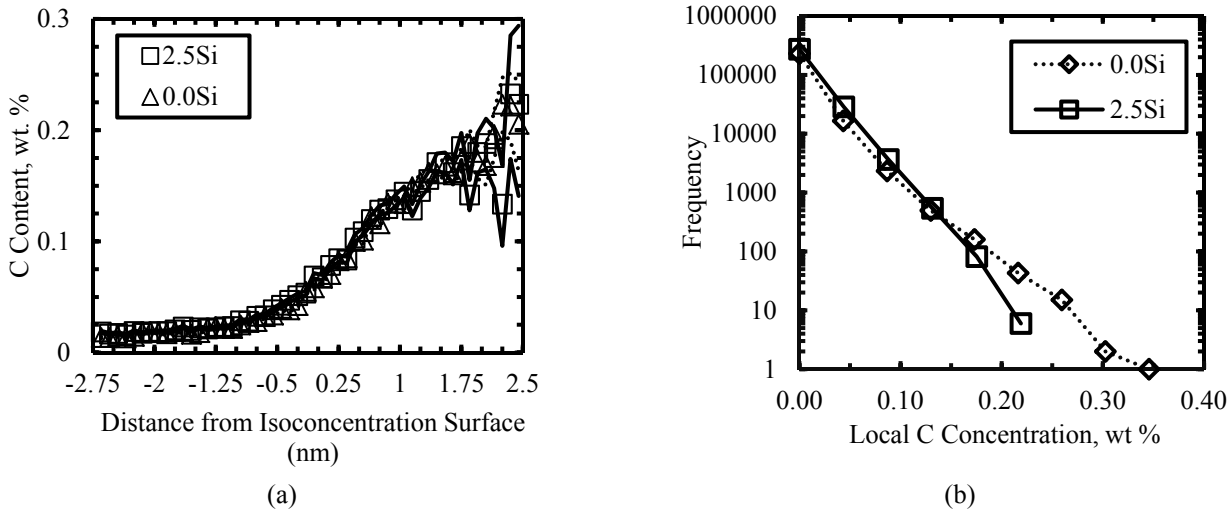

Figure 8. Proximity histogram: (a) C concentrations as a function of distance from the iso-concentration surface[20, 21]. Frequency of regions with given C Concentration (b) for the 0.0Si and 2.5Si tips.

DISCUSSION

As-Quenched Martensite Strength

In order to understand the effect Si has on strength, all differences in strengthening contributions between the 0.0Si alloy and the desired Si level must be quantified as shown in Equation 2.

$$\partial\sigma_M = \partial\sigma_{Fe} + \partial\sigma_{SS,Sub} + \partial\sigma_{DD} + \partial\sigma_{Lath} + \partial\sigma_{SS,C} + \partial\sigma_{PAGS} \quad (2)$$

For the following discussion, the effect of Si is considered as the difference in strength between the predicted value from Equation 2 and the actual strength. The differences in strengthening contributions from σ_{Fe} and $\sigma_{SS,Sub}$ are assumed to be constant between the alloys since the difference in substitutional composition is minuet. The next strengthening contribution considered, dislocation density, is dependent on quench rate, C content, and martensite start temperature[22, 23]. It is assumed that $\partial\sigma_{DD}$ is zero since these factors were kept as uniform as possible. Examination of the microstructure of the 0.0Si and 2.5Si showed that even between the alloys with the largest difference in Si content, there was no difference in lath size, which leads to $\partial\sigma_{Lath}$ value equal to zero. This allows equation 2 to be reduced to:

$$\partial\sigma_M = \partial\sigma_{SS,c} + \partial\sigma_{PAGS} \quad (3)$$

so that differences in martensite strength are dependent on differences in C content and PAGS in compared samples. The YS of low C martensite was experimentally determined by Winchell and Cohen to be:

$$\sigma_{SS,C}\ (\text{MPa}) = (1171\ ) \times (C)^{1/3} \quad (4)$$

where $\sigma_{SS,C}$ is in MPa and C is the C content of the martensite[24]. For simplicity, this is taken as the bulk C content. There is no known quantitative definition of the value of the final strengthening contribution by PAGS, σ_{PAGS}, for low C martensitic steels. However, the relationship of YS of martensite as a function of packet size (PS) has been developed by Swarr and Krauss as[25, 26]:

$$\sigma_{\text{Mart., PS}}\ (\text{MPa}) = 2209*(\text{PS})^{1/2}\ \text{MPa} \quad (5)$$

In turn, there is very strong relationship of PS and PAGS as demonstrated in Figure 9. Therefore, PAGS can be related to YS by (6:

$$\sigma_{PAGS}\ (\text{MPa}) = 2209 \times (2.6 \times PAGS - 0.82)^{1/2} \quad (6)$$

Substituting equations 4 and 6 into 3 and integrating from the 0.0Si to the any of the other alloy, x.xSi, it is possible to come to the functional form:

$$\sigma_{NM}\ (\text{MPa}) = (1171\ ) \times ((C_{x.xSi})^{\frac{1}{3}} - (C_{0.0Si})^{\frac{1}{3}}) + 2209 \times ((2.6 \times PAGS_{\text{x.xSi}} - 0.82)^{1/2} - (2.6 \times PAGS_{0.0\text{Si}} - 0.82)^{1/2}) \quad (7)$$

Equation 7 includes all possible strengthening mechanisms in investigated AQ martensite, excluding the strengthening contribution from Si additions. The actual YS and normalized value σ_{NM} are plotted in Figure 10 (a). The values for the 0.0Si condition are exactly the same since the strength is normalized to the 0.0Si strengthening conditions. As the Si content is increased, the strength of the σ_{NM} decreases by increasing amounts. The difference between the actual YS and σ_{NM} YS gives a quantitative evaluation of strengthening martensite by Si additions plotted in Figure 10 (b) as a function of Si content. The values of TS are plotted using the experimental average of the yield to tensile ratio of 0.775. It provides strengthening rate of 104 and 170 MPa/wt. % Si for YS and TS, respectively. This Si strengthening rate in martensite is quite similar to Si solid solution hardening in ferrite[27, 28].

There appears to be no difference in matrix strengthening due to C, that has not been accounted for by σ_{NM}, between the 0Si and 2.5Si since there are no differences in C clustering and both alloys lack carbides in AQ martensite. The difference in Si does not generate microstructural difference in lath size and the difference in PAGS is incorporated into the model. Therefore, only possible mechanism of Si hardening in as quenched martensite is lattice distortion like Si solid solution hardening in ferrite since low carbon martensite has very similar crystal structure. Therefore, Si addition is a very effective way to increase strength in low C AQ martensite. In addition, an improvement in ductility is observed with Si addition as shown in Figure 1. A mechanistic understanding of ductility improvement requires further study.

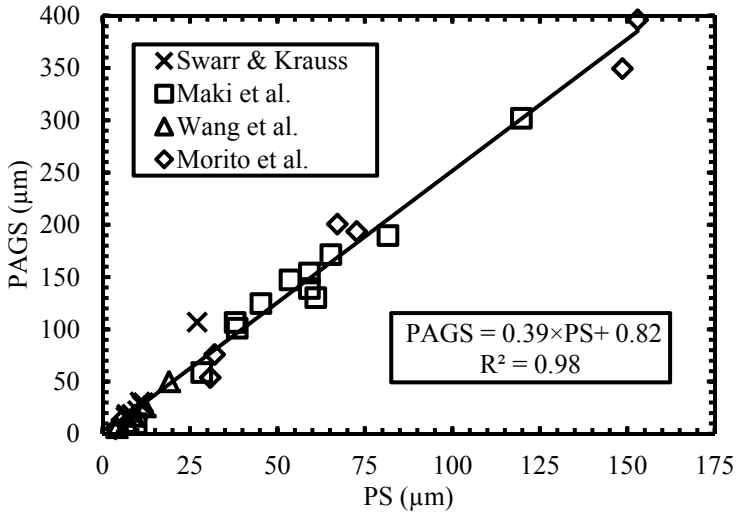

Figure 9. Relationship between martensite prior austenite grain size (PAGS) and packet size (PS) from literature[26, 29-31].

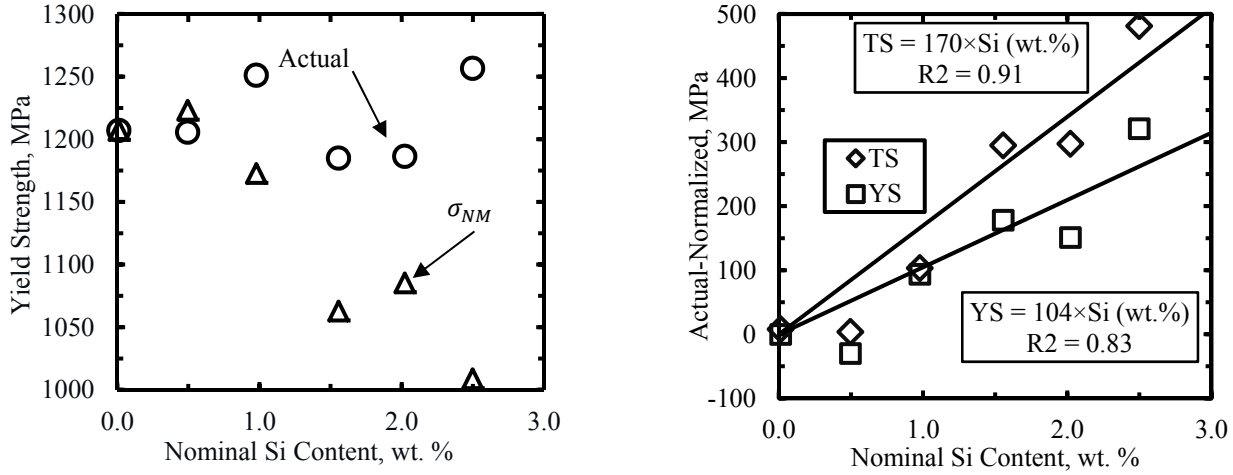

(a) (b)

Figure 10. The YS plotted as a function of nominal Si content for the actual tensile properties and the normalized tensile properties (a). Difference between the actual and normalized YS and converted TS plotted as a function of nominal Si content (b).

Quenched and Tempered Martensite

The addition of Si in low C martensite retards temper softening. Similar tempering behavior, in regards to TS, has been observed in martensite with higher C contents [10, 11, 15, 17, 18]. The TS is plotted as a function of Si content in Figure 11 (a) for the AQ samples and samples tempered at temperatures of 250 and 420 ºC. Figure 11 (a)shows that the degree of temper softening is reduced at Si content increases. There is a relatively uniform decrease of approximately 100 MPa from the AQ strength when the martensite is tempered at 250 ºC for all Si contents. When the tempering temperature is increased, significant softening occurs at lower Si contents. In the 0.0Si tempered martensite, elongated temper carbides are observed at the 250 ºC and 420 ºC temperatures (Figure 6). The size and amount are significantly increased at higher temperature. The large decrease in TS from the increased temper temperatures for the 0.0Si, as shown in Figure 11 (a), is likely the result of carbide coarsening which results in a lower C level in the martensite. The coarsening of carbides results in decreased carbide precipitation strengthening as well. At the higher Si level where tempering carbides are not formed (Figure 6), no significant decrease in TS is observed within investigated tempering temperatures and times. The effect of Si on property improvement of tempered martensite is not only limited to strength behavior. Figure 11 (b) demonstrates the effect of Si additions on the strength and ductility balance. As the tempering temperatures increases, low Si contents show significant reductions in strength and elongation when compared to the higher Si compositions.

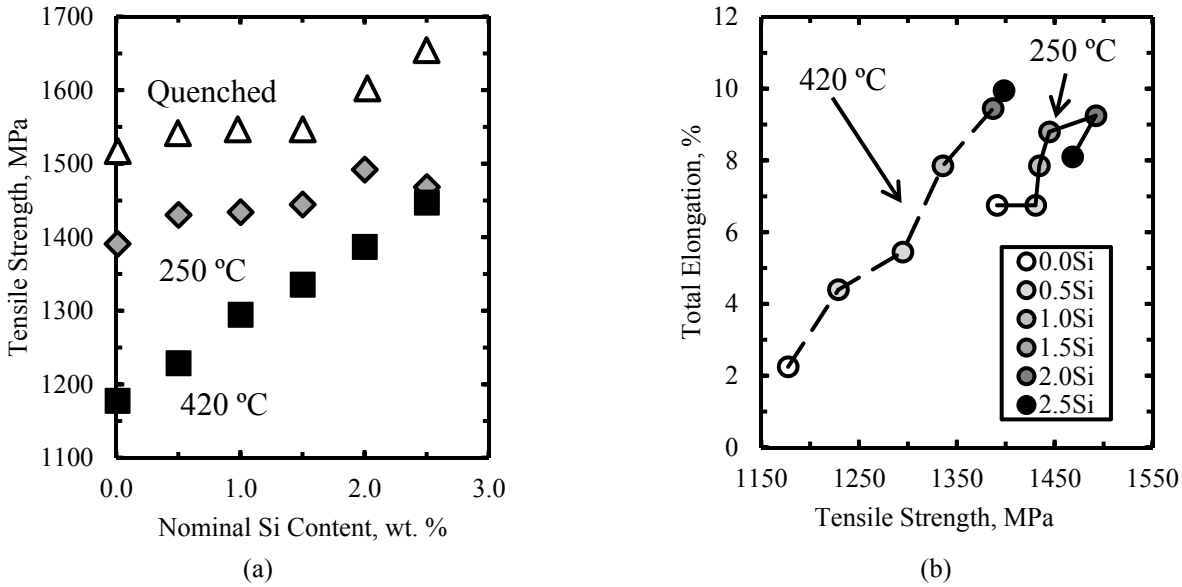

(a) (b)

Figure 11 – TS as a function of nominal Si content (a) is plotted for the Q&T martensite. The strength and ductility balance (b) for two tempering temperatures for the Si contents indicated.

CONCLUSIONS

1. A method was developed to distinguish strengthening contribution of specific factors through quantification of different strengthening mechanisms in low carbon as-quenched martensite.
2. The differences due to silicon additions in low carbon martensite influence not only the strength of the as-quenched martensite, but also the tempering response.
3. Atom probe tomography indicates that the presence of silicon does not have a significant influence on the formation of carbide and carbon clustering in as-quenched martensite.
4. In low carbon as-quenched martensite, after normalizing for additional strengthening mechanisms, silicon additions are shown to increase both yield and tensile strength. This strength increase is similar to the solid solution strengthening of silicon in ferrite (104 and 170 MPa/wt. % Si for yield and tensile strength, respectively).
5. With respect to tempering behavior, silicon additions decrease temper softening and reduce decreases in total elongation with tempering.
6. Increase in silicon improves the balance of tensile strength and total elongation of both as-quenched and quenched and tempered martensite.

REFERENCES

1. D. Matlock, J. Speer, “Design Considerations for the Next Generation of Advanced High Strength Sheet Steels,” in Proceedings of the 3rd International Conference on Structural Steels, Gyeongju, South Korea, August 22-24, 2006.
2. C. Horvath and J. Fekete, “Opportunities and Challenges for the Increased Usage of the Advanced High Strength Steels in Automotive Applications,” International Conference on Advanced High Strength Sheet Steels for Automotive Applications, Winter Park, Colorado, June 6-9, pp. 3-10, 2004 .
3. H. J. Jun and N. Fonstein, “Microstructure and Tensile Properties of TRIP-aided CR Sheet Steels : TRIP Dual and Q & P,” in *International Conference on New Developments in Advanced High-Strength Sheet Steels*, 2008, pp. 155–168.
4. C. Federici, S. Maggi, and S. Rigoni, “The Use of Advanced High Strength Steel Sheets in the Automotive Industry,” in *Super-High Strength Steels*, 2005, vol. 2012.
5. K. Sugimoto, “Ultra High-Strength Low-Alloy TRIP-Aided Sheet Steels with Bainitic Ferrite Matrix,” in International Conference on Advanced High Strength Sheet Steels for Automotive Applications Proceedings, 2004, vol. 2, pp. 63–70.
6. K. Sugimoto, B. Yu, Y. Mukai, and S. Ikeda, “Microstructure and Formability of Aluminum Bearing TRIP-Aided Steels with Annealed Martensite Matrix,” *ISIJ International*, vol. 45, no. 8, pp. 1194–1200, 2005.

7. P. Shanmugam and K. R. Karthikeyan, “Dual Phase Steel Tubes for Automotive Applications,” in *International Conference on Advanced High Strength Sheet Steels for Automotive Applications Proceedings*, 2004, pp. 171–178.
8. P. Winchell, M. Cohen, “The Strength of Martensite,” *Transactions of the ASM*, vol. 55, pp. 347-361, 1962.
9. G. R. Speich and P. R. Swann, “Yield Strength and Transformation of Quenched Iron-Nickel Alloys,” *J. Iron Steel Inst*., vol. 203, pp. 480-485, 1965.
10. A. G. Allten and P. Payson, “The Effect of Silicon on the tempering of Martensite,” *Transactions of the ASM*, vol. 45, pp. 498–525, 1953.
11. W. Owen, “The Effect of Silicon on the Kinetics of Tempering,” *Transactions of the ASM*, vol. 46, pp. 812–828, 1954.
12. S. S. Babu, K. Hono, and T. Sakurai, “Atom Probe Field Ion Microscopy Study of the Partitioning of Substitutional Elements during Tempering of a Low-Alloy Steel Martensite,” *Metallurgical and Materials Transactions A*, vol. 25, no. March, pp. 499–508, 1994.
13. G. Miyamoto, J. Oh, K. Hono, T. Furuhara, and T. Maki, “Effect of Partitioning of Mn and Si on the Growth Kinetics of Cementite in Tempered Fe–0.6 mass% C Martensite,” *Acta Materialia*, vol. 55, no. 15, pp. 5027–5038, 2007.
14. S. Ghosh, “Rate-Controlling Parameters in the Coarsening Kinetics of Cementite in Fe–0.6C Steels During Tempering,” *Scripta Materialia*, vol. 63, no. 3, pp. 273–276, Aug. 2010.
15. W. J. Nam and H. C. Choi, “Effect of Si on mechanical properties of low alloy steels,” *Materials Science and Technology*, vol. 15, pp. 527-530, 1999.
16. J. P. Naylor, “The Influence of the Lath Morphology on the Yield Stress and Transition Temperature of Martensitic-Bainitic Steels,” *Metallurgical Transactions A*, vol. 10, pp. 861-873, 1979.
17. J. Gordine and I. Codd, “The Influence of Silicon up to 1.5 wt-% on the Tempering Characteristics of a Spring Steel,” *Journal of The Iron and Steel Institute*, pp. 461–467, 1969.
18. C. H. Shih, B. L. Averbach, M Cohen, “Some Effects of Silicon on the Mechanical Properties of High Strength Steels,” *Transactions of the ASM,* vol. 48, pp. 86-115, 1956.
19. “Standard Test Methods for Determining Average Grain Size,” ASTM International. E112-10.
20. O. C. Hellman, J. B. du Rivage, and D. N. Seidman, “Efficient Sampling for Three-Dimensional Atom Probe Microscopy Data,” *Ultramicroscopy*, vol. 95, pp. 199–205, 2003.
21. O. Hellman, J. Vandenbroucke, J. Blatz du Rivage, and D. N. Seidman, “Application Software for Data Analysis for Three-Dimensional Atom Probe Microscopy,” *Materials Science and Engineering: A*, vol. 327, pp. 29–33, Apr. 2002.
22. G. Ansell, S. Donachie, and R. Messler, “The Effect of Quench Rate on the Martensitic Transformation in Fe-C Alloys,” *Metallurgical Transactions A*, vol. 2, pp. 2443–2449, 1971.
23. L. A. Norström, “On the Yield Strength of Quenched Low-Carbon Lath Martensite,” *Scandinavian Journal of Metallurgy*, vol. 5, pp. 159-165, 1976.
24. P. G. Winchell and M Cohen, in: G. Thomas, J. Washburn (Eds.), *Electron Microscopy and Strength of Crystals*, Interscience, 1963, p.995.
25. T. Swarr and G. Krauss, “Boundaries and the Strength of Low Carbon Ferrous Martensites,” *Grain Boundaries in Engineering Materials*, pp. 127-138, 1974.
26. T. Swarr and G. Krauss, “The Effect of Structure on the Deformation of As-Quenched and Tempered Martensite in an Fe-0.2 Pct C Alloy,” *Metallurgical Transactions A*, vol. 7, pp. 41-48, 1976.
27. A. Uenishi, C. Teodosiu, “Solid Solution Softening at High Strain Rates in Si- and/or Mn-added Interstitial Free Steels,” *Acta Materialia*, vol. 51, no. 15, pp. 4437-4446, 2003.
28. W. C. Leslie, Iron and its Dilute Substitutional Solid Solutions,” *Metallurgical Transactions*, vol. 3, pp. 5-26, 1972.
29. T. Maki, K. Tsuzaki, I. Tamura, “The Morphology of Microstructure Composed of Lath Martensites in Steels,” *Transactions ISIJ*, vol. 20, pp. 207-214, 1990.
30. C. Wang, M. Wang, J. Shi, W. Hui, H. Dong, “Effect of Microstructure Refinement on the Strength and Toughness of Low Alloy Martensitic Steel,” *J. Mater. Sci. Tech.*, vol. 23, pp. 659-664, 2007.
31. S. Morito, H. Saito, T. Ogawa, T. Furuhara, and T. Maki, “Effect of Austenite Grain size on the Morphology and Crystallography of Lath Martensite in Low Carbon Steels,” *ISIJ international*, vol. 45, no. 1, pp. 91–94, 2005.